THE JOURNAL OF PHYSICAL CHEMISTRY A

pubs.acs.org/JPCA Article

Spin-Crossover from a Well-Behaved, Low-Cost meta-GGA Density Functional

Daniel Mejía-Rodríguez* and S. B. Trickey*

Cite This: J. Phys. Chem. A 2020, 124, 9889–9894 Read Online

ACCESS | Metrics & More | Article Recommendations | Supporting Information

ABSTRACT: The recent major modification, r^{2}SCAN, of the SCAN (strongly constrained and appropriately normed) meta-GGA exchange-correlation functional is shown to give substantially better spin-crossover electronic energies (high spin minus low spin) on a benchmark data set than the original SCAN as well as on some Fe complexes. The deorbitalized counterpart r^{2}SCAN-L is almost as good as SCAN and much faster in periodically bounded systems. A combination strategy for the balanced treatment of molecular and periodic spin-crossover therefore is recommended.

INTRODUCTION

Context. The essential physical trait of a spin-crossover (SCO) molecule is a small energy difference between the ground state of one spin and an excited state of a different spin. Small in this context typically means a few kcal/mol (i.e., a few hundred meV). Calculation of such differences is challenging. An added challenge is that spin-crossover is of greatest interest in condensed phases. The interest arises both because of the intrinsic complexity of bistability and because of its importance for functional materials in technological applications such as switchable-spin memories. For an early treatment see ref 1, and for a very recent one see ref 2. Predictive calculation protocols therefore must be equally accurate for both isolated molecules and their condensed phases.

Meeting that challenge has been difficult. It is not our purpose to survey the literature. For that, see refs 3−11 The last-mentioned of these is particularly relevant. It presented a database of 20 molecules in which SCO arises from a first-row transition metal. Against that database, the authors of ref 11 tested several rather sophisticated density functional approximations (DFAs) for exchange and correlation (XC) and concluded that the hybrid Tao−Perdew−Staroverov−Scuseria (TPSSh)[12,13] DFA was best overall.

The focus on DFAs stems from the need for affordable calculations both on large molecules and on their condensed aggregates. Refined wave function methods are applicable, though costly, in SCO molecules. They are prohibitively costly in the condensed phases. In principle, density functional theory (DFT) methods should be applicable to both. Until recently, however, all affordable, "lower-rung"[14] DFAs have exhibited bias to either the molecular or the condensed side.

The recommendation of TPSSh is itself somewhat problematic. The drawback that is relevant here is its hybrid character, namely, inclusion of 10% single-determinant exchange (often inaccurately called Hartree−Fock or exact exchange; both terms have precise, well-defined meanings that are not met by a hybrid DFA).

The nonhybrid antecedent of TPSSh, TPSS, is a meta-Generalized Gradient Approximation (meta-GGA). In meta-GGAs, chemically distinct electron density inhomogeneities are recognized by the use of so-called indicator functions. In the case of TPSS there are two. Based on their values, the meta-GGA switches between a nonempirical GGA DFA that is constructed to work well with molecular-like environments and another for condensed-phase environments.

Largely for reasons of accuracy, TPSS has been supplanted by a more refined meta-GGA called SCAN, for "strongly constrained and appropriately normed".[15,16] It uses only one indicator function, denoted $\alpha(\mathbf{r})$. With comparatively few exceptions (e.g., ref 17), SCAN has proven successful in predicting a wide variety of molecular and condensed-phase properties. That success is a consequence of the physical realism associated with the enforcement in SCAN of all the rigorous constraints that a meta-GGA can meet, along with calibration to the energies of selected primitive physical systems (the "appropriate norms"; see the Supporting Information to ref 15).

SCAN and Spin-Crossover. Motivated by other successful uses of SCAN, Cirera and Ruiz[18] tested it recently against the 20-molecule SCO database of ref 11. Their conclusion was that SCAN "...gives the right ground state for the whole set of test cases" and is "...the unique pure DFT functional to provide with comparable results for such a challenging test." All of the systems

Received: September 30, 2020
Revised: October 29, 2020
Published: November 11, 2020

https://dx.doi.org/10.1021/acs.jpca.0c08883
J. Phys. Chem. A 2020, 124, 9889−9894

have low-spin (LS) as the ground state, as indeed is found by SCAN. However, the SCO energy differences,

$$\Delta E_{HL} := E_H - E_L \quad (1)$$

with E_H (E_L) the high-spin (low-spin) total energy, from SCAN are only semiquantitative at best. In some cases they are off by as much as a factor of 2 or more. Note that these comparisons were with respect to TPSSh results for ΔE_{HL}. Those values themselves lead to an overestimation of the crossover temperature.[11] A technical difficulty is that SCAN calculations required dense radial integration grids. An uncomfortable aspect is that the best range of ΔE_{HL} values from SCAN were generated with a suboptimal (not fully converged) grid.

Grid density and SCF convergence difficulties with SCAN already had become well-known among practitioners. Those problems were addressed by Bartók and Yates[19] with regularized SCAN (rSCAN). It refined α and smoothed the SCAN switching function to yield improved computational behavior. Though rSCAN preserves the good molecular bond lengths and vibrational frequencies given by SCAN, it sacrifices the SCAN performance for benchmark molecular heats of formation.[20] In periodic solids, SCAN and rSCAN are about the same for lattice constants and cohesive energies[20] on a 55 solid test set[21] and for bulk moduli on a 44 solid set.[22]

Very recently Furness et al.[23] have cured the deficiencies of rSCAN by constructing a similar regularization that restores all but one of the constraints satisfied by SCAN but violated by rSCAN. The regularized-restored SCAN functional (r^{2}SCAN) that results combines the strong performance trends of SCAN relative to molecular and solid data sets with the numerical stability of rSCAN.

A separate conceptual and computational issue of meta-GGAs in general is their explicit dependence upon the Kohn−Sham (KS) orbitals. As a matter of practice, the computational costs from that dependence lead to the use of the generalized KS (gKS) equations rather than the multiplicative potential of the ordinary KS equation. There is both a difference of content[24,25] and a computational cost penalty for gKS compared to KS. We had addressed both those issues by deorbitalization, that is, the replacement of the orbital dependence with a function of the density, its gradient, and its Laplacian. That gave the SCAN-L DFA.[26,27] Except for elemental 3d magnetic solids, SCAN-L delivered essentially the same performance as SCAN. It should be faster than SCAN, but in practice numerical instabilities caused very slow SCF convergence. Very recently we found that the greatly improved numerical stability of r^{2}SCAN is preserved under deorbitalization to yield r^{2}SCAN-L. In solid calculations, it runs almost four times faster than r^{2}SCAN.[28]

The advent of r^{2}SCAN and r^{2}SCAN-L makes it imperative to investigate their SCO performance on the ref 11 data set to see if the changes from SCAN and SCAN-L (respectively) affect the delicate energy differences involved.

We note that validation and testing of any DFA with regard to SCO must be preceded by standard screening. Any plausible DFA candidate for SCO first must have given acceptable accuracy for molecular dissociation energies, bond lengths, and fundamental vibrational frequencies and must give acceptable crystal structures, cohesive energies, and bulk moduli, all against widely used databases. If the fundamental molecular vibration frequencies and bulk moduli are of decent quality, it is plausible that the enthalpic contributions to the SCO temperature $T_{1/2}$ will be reasonable. Notice that the *essential* untested ingredient from routine DFA screening is ΔE_{HL}. If the candidate DFA delivers bad values for that difference, the only way it could deliver good $T_{1/2}$ values would be by compensating error, i.e., right answers for wrong reasons. We focus therefore on ΔE_{HL}. For the sake of delineating DFA performance in difficult spin systems, we also study the Cr_2 dissociation curve.

COMPUTATIONAL METHODS

Molecular calculations were done with a locally modified developers' version of the NWChem code[29] using the unrestricted KS procedure, the def2-TZVP basis set[30] in spherical representation, and the FINE numerical integration grid. The number of radial shells and the corresponding Lebedev angular points[31−36] per radial shell vary depending on the atom type, as shown in Table 1. Previously we have shown that this grid density is good enough to integrate both r^{2}SCAN and r^{2}SCAN-L XC potentials and energies.[28] SCAN calculations used a custom-defined grid with 200 radial shells and 590 angular points per shell.

Table 1. Number of Radial and Lebedev Angular Points Present in the NWChem FINE Grid Preset

element	radial shells	angular points
H	60	590
B, C, N, O	70	590
P, S	123	770
Cr, Mn, Fe, Co, Br	140	974
I	141	974

Moreover, all calculations used Weigend's Coulomb-fitting basis set[37] for the density fitting scheme.[38,39] Default options for guess density, convergence stabilization and acceleration techniques, and convergence criteria for both electronic and ionic relaxations were used.

The D3(BJ)[40,41] empirical dispersion correction, with parameters optimized for SCAN,[42] was tried as an exploratory step. We remark that both r^{2}SCAN and r^{2}SCAN-L should include some midrange dispersion by construction, so the D3(BJ) corrections are rather small.

Nine SCO systems in the Cirera−Via-Nadal−Ruiz database[11] database are positively charged (2 Mn^{III}, 3 Fe^{III}, 1 Fe^{II}, and 3 Co^{II}). None of the counterions were included in the calculations. That choice is consistent with the original database and, as well, avoids the intrinsic bias toward noncharged species in the gas phase. The omission corresponds to removal of 10% or less of the total atomic count for most of the charged complexes. However, the 45 atoms of the tetraphenyl borate anion originally present in the Fe^{III} system labeled S9 account for almost 40% of the total number of atoms of that system.

The spin-state energetics for the four Fe complexes, three Fe^{III} and one Fe^{II}, recently benchmarked by Radoń[43] also were computed. Geometries of all four were reoptimized under the same symmetry constraints as in ref 43 using the same settings as for systems in the ref 11 database.

The chromium dimer potential energy curves were obtained using a modified version of VASP 5.4.4[44−47] using the 14-electron projector augmented-wave (PAW) data set.[48,49] The dimer was aligned along the z-axis inside a large $12 \times 12 \times 15$ Å^3 box. The calculations used the *accurate* precision setting and a 600 eV kinetic energy cutoff and included aspherical corrections inside the PAW spheres.

https://dx.doi.org/10.1021/acs.jpca.0c08883
J. Phys. Chem. A 2020, 124, 9889−9894

Table 2. High-Spin to Low-Spin ΔE_{HL} Energies (kcal/mol)[a]

system	TPSSh[b]	SCAN[b]	SCAN[c]	rSCAN	r^{2}SCAN	r^{2}SCAN+D3	r^{2}SCAN-L
S1	6.54	11.49	7.98	2.93	3.36	4.14	10.54
S2	4.27	8.06	8.94	3.27	3.09	3.07	11.55
S3	5.53	8.54	8.41	3.69	3.45	3.58	19.39
S4	4.12	7.21	7.32	2.04	2.40	2.07	10.42
S5	11.19	10.08	10.93	−2.27	5.06	4.92	12.49
S6	10.67	10.39	11.07	5.24	4.57	4.77	19.52
S7	9.40	10.19	11.19	5.16	4.51	4.83	19.70
S8	9.78	11.29	11.63	3.21	2.92	3.07	18.51
S9	11.45	17.61	18.74	10.42	10.17	10.62	25.79
S10	10.69	14.28	14.90	5.76	5.48	6.02	20.52
S11	6.13	13.50	14.31	−26.43	5.23	4.52	18.01
S12	8.53	16.85	16.69	−54.07	6.34	6.46	19.01
S13	9.31	20.41	20.76	−15.64	10.06	10.86	22.65
S14	9.36	23.22	21.13	−19.95	9.91	10.60	22.90
S15	5.00	11.75	14.01	−28.96	2.97	3.07	15.37
S16	3.00	10.44	12.30	7.90	6.40	6.84	13.68
S17	2.29	8.34	14.53	10.16	3.43	3.70	10.29
S18	2.14	10.08	10.17	6.31	5.77	7.28	13.11
S19	3.78	11.80	14.15	10.22	8.99	10.69	17.95
S20	6.59	10.06	10.76	6.80	6.41	6.90	13.62

[a]Systems are labeled as in Cirera and Ruiz.[18] [b]From ref 18. [c]This work.

RESULTS AND DISCUSSION

Table 2 and Figure 1 show ΔE_{HL}, in kcal/mol, obtained with SCAN, rSCAN, r^{2}SCAN, and r^{2}SCAN-L. Results from ref 18 for

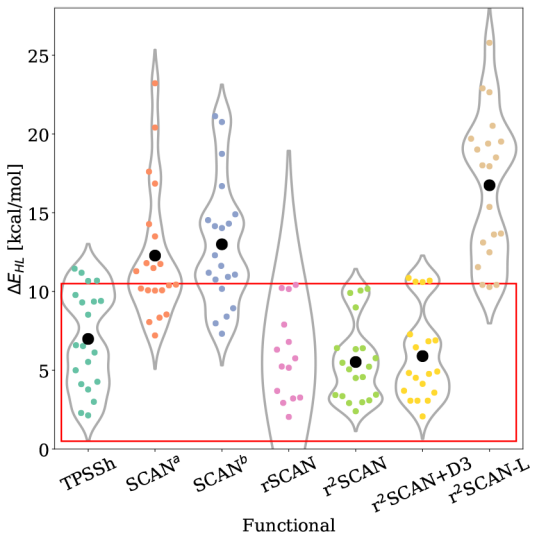

Figure 1. Electronic low-spin−high-spin energy differences ΔE_{HL} in kcal/mol. The colored dots correspond to the actual individual results, while the large black dot corresponds to the mean ΔE_{HL} obtained with each functional. The red box is the same as used in ref 18 to indicate the region where the electronic energy difference can be compensated by the entropy in usual SCO systems. Note that the rSCAN violin was cut in order to enhance the visibility of other results. TPSSh and SCAN[a] are from ref 18. All other are this work.

TPSSh and SCAN are included for comparison. SCAN results correspond to the denser numerical integration grid (SG-2) which is made up of 75 radial shells with 302 Lebedev angular points per shell. Our ΔE_{HL} values obtained with SCAN are around 1.5 kcal/mol from those of ref 18. This difference was expected based on our previous studies (see refs 20 and 28).

Reassuringly, r^{2}SCAN gives the correct low-spin configuration for the ground state for all 20 complexes, with all ΔE_{HL} values inside a 10 kcal/mol energy window proposed by Cirera and Ruiz (compare Figure 1 with Figure 3 of ref 18). Also striking is the fact that the r^{2}SCAN DFA yields a marked reduction of the predicted ΔE_{HL} compared to SCAN. The r^{2}SCAN values are, in fact, slightly smaller than those predicted by the DFA hybrid TPSSh.

In contrast, the deorbitalized version, r^{2}SCAN-L, gives ΔE_{HL} larger than, but still comparable to, the values obtained with SCAN. The advantage of r^{2}SCAN-L is mainly the potential speedup one can achieve by means of its local multiplicative potential. We return to this point below.

Table 2 also shows that the inclusion of empirical dispersion corrections via the DFT-D3 approach[40,41] changes ΔE_{HL} values by about 0.5 kcal/mol, with larger effects for the Co systems. We stress that forces from the r^{2}SCAN+D3 combination were included during geometry optimizations. We did not find unrealistic geometries such as reported in ref 11. Larger effects generally are seen when the DFT-D3 correction is used only for single-point energies at the corresponding uncorrected DFA minima (see for example ref 18).

In order to obtain further insight about the specific changes that lead to the drastic performance differences among these closely related DFAs, we also tried rSCAN calculations. As Figure 1 and Table 2 show, rSCAN does almost as well as r^{2}SCAN for the majority of systems but gives the wrong sign for six of them. The most notable failures occur in Fe^{II} d^6 systems (S11−S15). In them, rSCAN overstabilizes the high-spin state by as much as 54 kcal/mol.

It is interesting to note that, barring rSCAN results for Fe(II) systems, the S9 ΔE_{HL} is the largest of the set for the TPSSh, r^{2}SCAN, r^{2}SCAN-L, and rSCAN DFAs. This may be a direct consequence of the effects that the missing counterion can have on the overall structure and energetics of the complex (see Computational Methods), but investigation of the issue is outside the scope of this work.

https://dx.doi.org/10.1021/acs.jpca.0c08883
J. Phys. Chem. A 2020, 124, 9889−9894

For thoroughness, we augmented the 20-system data set with the four systems proposed by Radoń in ref 43. Radoń gave ΔE_{HL} values by removing environmental effects from experimental data in order to have a straightforward reference for comparison. Table 3 shows ΔE_{HL} values for those systems (labeled as S21−S24) and the corresponding reference reported as extrapolated from experiment. Note that system S24 is the same as S8 reported in Table 2. The TPSSh and TPSSh+D3 values taken from ref 43 are from nonrelativistic calculations without corrections for spin contamination. Also note that ΔE_{HL} for S21 and S22 corresponds to vertical excitation energies, so the DFT-D3 corrected and uncorrected values are exactly the same. Again, we see that r^{2}SCAN gives the correct sign and outperforms TPSSh(+D3).

Table 3. High-Spin to Low-Spin ΔE_{HL} Energies (kcal/mol) of Complexes S21−S24

	S21	S22	S23	S24 (S8)
TPSSh[a]	−29.2	24.7	7.6	10.8
TPSSh+D3[a]	−29.2	24.7	8.3	10.2
r^{2}SCAN	−45.4	22.4	6.8	2.9
exptl[a]	−47.4	19.7	3.8	2.4

[a]Nonrelativistic values from ref 43.

Based on the foregoing results, we can summarize our findings as follows:

- The reduced ΔE_{HL} values (compared to those from SCAN) obtained with rSCAN and r^{2}SCAN mean that the seemingly small changes made in the SCAN switching function are responsible for the majority of the effects.
- The failures obtained from rSCAN but not with r^{2}SCAN highlight the importance that constraint satisfaction has in ensuring the maximum scope of validity for a given DFA.
- The larger ΔE_{HL} values obtained with SCAN-L and r^{2}SCAN-L also illuminate the importance of the switching function in the prediction of spin-state energetics. Although the deorbitalization procedure[26,27] does not change the switching function *directly*, the differences between the approximated iso-orbital indicator α_L and the original one modify, indirectly, its behavior.[17]

CONCLUSIONS AND OUTLOOK

We have shown that the r^{2}SCAN DFA provides a quantitatively correct ground state for all molecules in the SCO database put forth in ref 11 as well as on the four Fe complexes in ref 43. Furthermore, r^{2}SCAN apparently is the only comparatively simple DFA, including hybrid ones, that gives all high-spin to low-spin energy differences Δ_{HL} inside what is believed to be the appropriate energy range. On the basis of that accuracy and comparatively modest computational costs, we therefore recommend, strongly, the use of r^{2}SCAN to describe 3d SCO systems.

Though the accuracy for ΔE_{HL} provided by the deorbitalized version, r^{2}SCAN-L, is not as good as what r^{2}SCAN gives, it is useful that r^{2}SCAN-L does perform on par with the accuracy from the original SCAN but without the numerical integration issues. The advantage of r^{2}SCAN-L is its substantially lower computational costs in codes that use fast-Fourier transforms to obtain the appropriate derivatives of the density. In those codes, the local multiplicative potential of r^{2}SCAN-L can achieve calculations as much as four times faster than with r^{2}SCAN. That provides a major opportunity. The key to it is that the sacrifice in bond length and vibrational frequency accuracy in going from r^{2}SCAN to r^{2}SCAN-L is much smaller than the ΔE_{HL} accuracy sacrifice. The strategy we recommend therefore is to do geometry optimizations (either molecular or solid) with r^{2}SCAN-L and then do a single -point calculation with r^{2}SCAN to determine ΔE_{HL}. We have that strategy under investigation but point out that an analogous approach, using SCAN and SCAN-L, has proven to be successful.[50]

While r^{2}SCAN is much better for SCO on the Cirera−Via−Nadal−Ruiz and Radoń data sets and therefore we recommend it, we do so with caution. r^{2}SCAN is not perfect for magnetization nor is r^{2}SCAN-L. See Figure 2 for a comparison of r^{2}SCAN and r^{2}SCAN-L results with those from other DFAs for the famously difficult case of Cr_2 dissociation, an issue recently readdressed in ref 51. (Note that the corresponding figure in ref 51 displays the experimental data incorrectly by a factor of 2.) The reasons for the superior performance of the GGA functional PBE compared to any of the meta-GGA functionals on this system remain obscure to us and to other DFA developers (John Perdew, private communication). Another aspect of the obscurity is that, distinct from SCAN, r^{2}SCAN and both deorbitalized functionals do not magnetize benzene or graphene. This slight improvement is also seen in the solid phase, since both r^{2}SCAN and r^{2}SCAN-L improve upon SCAN (see Table 3 of ref 28). Caution is still warranted in the use of r^{2}SCAN and r^{2}SCAN-L according to the protocol we have proposed here.

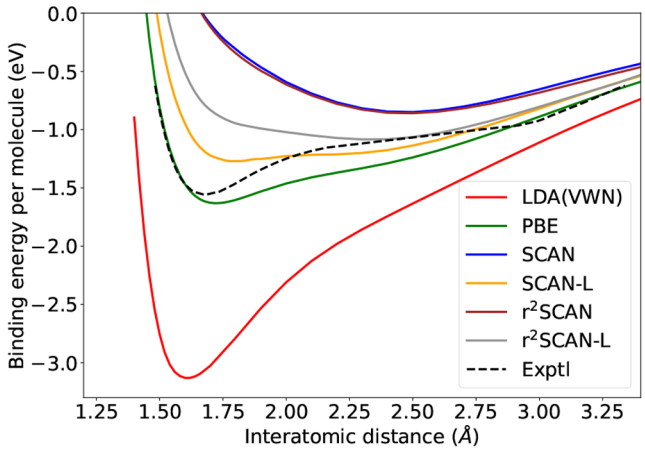

Figure 2. Cr_2 potential energy curve (eV) obtained with six different DFAs in VASP. The experimental curve is reproduced from ref 52 assuming that the bottom of the well is at −1.56 eV.[53,54]

ASSOCIATED CONTENT

Supporting Information

The Supporting Information is available free of charge at https://pubs.acs.org/doi/10.1021/acs.jpca.0c08883.

r^{2}SCAN optimized structures for the 23 complexes studied (ZIP)

Chemical formulas for the 23 complexes studied (PDF)

AUTHOR INFORMATION

Corresponding Authors

Daniel Mejía-Rodríguez − *Center for Molecular Magnetic Quantum Materials, Quantum Theory Project, Department of*

https://dx.doi.org/10.1021/acs.jpca.0c08883
J. Phys. Chem. A 2020, 124, 9889−9894

Physics, University of Florida, Gainesville, Florida 32611, United States; orcid.org/0000-0002-0350-2941; Email: dmejiarodriguez@ufl.edu

S. B. Trickey − *Center for Molecular Magnetic Quantum Materials, Quantum Theory Project, Department of Physics, University of Florida, Gainesville, Florida 32611, United States;* orcid.org/0000-0001-9224-6304; Email: trickey@qtp.ufl.edu

Complete contact information is available at: https://pubs.acs.org/10.1021/acs.jpca.0c08883

Notes

The authors declare no competing financial interest.

■ ACKNOWLEDGMENTS

This work was supported by U.S. Dept. of Energy under Energy Frontier Research Center grant DE-SC 0019330.

■ REFERENCES

(1) Kahn, O.; Kröber, J.; Jay, C. Spin transition molecular materials for displays and data recording. *Adv. Mater.* **1992**, *4*, 718−728.
(2) Senthil Kumar, K.; Šalitroš, I.; Heinrich, B.; Moldovan, S.; Mauro, M.; Ruben, M. Spin-crossover in iron(II)-phenylene ethynylene-2,6-di(pyrazol-1-yl) pyridine hybrids: toward switchable molecular wire-like architectures. *J. Phys.: Condens. Matter* **2020**, *32*, 204002.
(3) Ioannidis, E. I.; Kulik, H. J. Towards quantifying the role of exact exchange in predictions of transition metal complex properties. *J. Chem. Phys.* **2015**, *143*, 034104.
(4) Mortensen, S. R.; Kepp, K. P. Spin propensities of octahedral complexes from density functional theory. *J. Phys. Chem. A* **2015**, *119*, 4041−4050.
(5) Cirera, J.; Ruiz, E. Theoretical modeling of the ligand-tuning effect over the transition temperature in four-coordinated Fe^{II} molecules. *Inorg. Chem.* **2016**, *55*, 1657−1663.
(6) Harding, D. J.; Harding, P.; Phonsri, W. Spin crossover in iron(III) complexes. *Coord. Chem. Rev.* **2016**, *313*, 38−61.
(7) Kepp, K. P. Theoretical study of spin crossover in 30 iron complexes. *Inorg. Chem.* **2016**, *55*, 2717−2727.
(8) Amabilino, S.; Deeth, R. J. DFT analysis of spin crossover in Mn(III) complexes: Is a two-electron $S = 2$ to $S = 0$ spin transition feasible? *Inorg. Chem.* **2017**, *56*, 2602−2613.
(9) Flores-Leonar, M. M.; Moreno-Esparza, R.; Ugalde-Saldıvar, V. M.; Amador-Bedolla, C. Correlating properties in iron(III) complexes: A DFT description of structure, redox potential and spin crossover phenomena. *ChemistrySelect* **2017**, *2*, 4717−4724.
(10) Sirirak, J.; Sertphon, D.; Phonsri, W.; Harding, P.; Harding, D. J. Comparison of density functionals for the study of the high spin low spin gap in Fe(III) spin crossover complexes. *Int. J. Quantum Chem.* **2017**, *117*, No. e25362.
(11) Cirera, J.; Via-Nadal, M.; Ruiz, E. Benchmarking density functional methods for calculation of state energies of first row spin-crossover molecules. *Inorg. Chem.* **2018**, *57*, 14097−14105.
(12) Staroverov, V. N.; Scuseria, G. E.; Tao, J.; Perdew, J. P. Comparative assessment of a new nonempirical density functional: Molecules and hydrogen-bonded complexes. *J. Chem. Phys.* **2003**, *119*, 12129.
(13) Tao, J.; Perdew, J. P.; Staroverov, V. N.; Scuseria, G. E. Climbing the density functional ladder: Nonempirical meta-generalized gradient approximation designed for molecules and solids. *Phys. Rev. Lett.* **2003**, *91*, 146401.
(14) Perdew, J. P.; Schmidt, K. Jacob's ladder of density functional approximations for the exchange-correlation energy. *AIP Conf. Proc.* **2000**, *577*, 1−20.
(15) Sun, J.; Ruzsinszky, A.; Perdew, J. P. Strongly constrained and appropriately normed semilocal density functional. *Phys. Rev. Lett.* **2015**, *115*, 36402.
(16) Sun, J.; Remsing, R. C.; Zhang, Y.; Sun, Z.; Ruzsinszky, A.; Peng, H.; Yang, Z.; Paul, A.; Waghmare, U.; Wu, X.; et al. Accurate first-principles structures and energies of diversely bonded systems from an efficient density functional. *Nat. Chem.* **2016**, *8*, 831−836.
(17) Mejía-Rodríguez, D.; Trickey, S. B. Analysis of over-magnetization of elemental transition metal solids from the SCAN density functional. *Phys. Rev. B: Condens. Matter Mater. Phys.* **2019**, *100*, No. 041113.
(18) Cirera, J.; Ruiz, E. Assessment of the SCAN functional for spin state energies in spin-crossover systems. *J. Phys. Chem. A* **2020**, *124*, 5053−5058.
(19) Bartók, A. P.; Yates, J. R. Regularized SCAN functional. *J. Chem. Phys.* **2019**, *150*, 161101.
(20) Mejía-Rodríguez, D.; Trickey, S. B. Comment on "Regularized SCAN functional" [J. Chem. Phys. 150, 161101 (2019)]. *J. Chem. Phys.* **2019**, *151*, 207101.
(21) Peng, H.; Yang, Z.-H.; Perdew, J. P.; Sun, J. Versatile van der Waals density functional based on a meta-generalized gradient approximation. *Phys. Rev. X* **2016**, *6*, 41005.
(22) Tran, F.; Stelzl, J.; Blaha, P. Rungs 1 to 4 of DFT Jacob's ladder: Extensive test on the lattice constant, bulk modulus, and cohesive energy of solids. *J. Chem. Phys.* **2016**, *144*, 204120.
(23) Furness, J. W.; Kaplan, A. D.; Ning, J.; Perdew, J. P.; Sun, J. Accurate and numerically efficient r^2SCAN meta-generalized gradient approximation. *J. Phys. Chem. Lett.* **2020**, *11*, 8208−8215.
(24) Yang, Z.-h.; Peng, H.; Sun, J.; Perdew, J. P. More realistic band gaps from meta-generalized gradient approximations: Only in a generalized Kohn-Sham scheme. *Phys. Rev. B: Condens. Matter Mater. Phys.* **2016**, *93*, 205205.
(25) Perdew, J.; Yang, W.; Burke, K.; Yang, Z.; Gross, E.; Scheffler, M.; Scuseria, G.; Henderson, T.; Zhang, I.; Ruzsinszky, A.; et al. Understanding band gaps of solids in generalized Kohn−Sham theory. *Proc. Natl. Acad. Sci. U. S. A.* **2017**, *114*, 2801−2806.
(26) Mejía-Rodríguez, D.; Trickey, S. B. Deorbitalization strategies for meta-generalized-gradient-approximation exchange-correlation functionals. *Phys. Rev. A: At., Mol., Opt. Phys.* **2017**, *96*, 052512.
(27) Mejía-Rodríguez, D.; Trickey, S. B. Deorbitalized meta-GGA exchange-correlation functionals in solids. *Phys. Rev. B: Condens. Matter Mater. Phys.* **2018**, *98*, 115161.
(28) Mejía-Rodríguez, D.; Trickey, S. B. Meta-GGA performance in solids at almost GGA cost. *Phys. Rev. B: Condens. Matter Mater. Phys.* **2020**, *102*, 121109.
(29) Aprà, E.; Bylaska, E. J.; de Jong, W. A.; Govind, N.; Kowalski, K.; Straatsma, T. P.; Valiev, M.; van Dam, H. J. J.; Alexeev, Y.; Anchell, J.; et al. NWChem: Past, present, and future. *J. Chem. Phys.* **2020**, *152*, 184102.
(30) Weigend, F.; Ahlrichs, R. Balanced basis sets of split valence, triple zeta valence and quadruple zeta valence quality for H to Rn: Design and assessment of accuracy. *Phys. Chem. Chem. Phys.* **2005**, *7*, 3297−3305.
(31) Lebedev, V. Values of the nodes and weights of quadrature formulas of Gauss-Markov type for a sphere from the ninth to seventeenth order of accuracy that are invariant with respect to an octahedron group with inversion. *Zh. Vychisl. Mater. Mater. Fiz.* **1975**, *15*, 48−54.
(32) Lebedev, V. Quadratures on the sphere. *Zh. Vychisl. Mater. Mater. Fiz.* **1976**, *16*, 293−306.
(33) Lebedev, V. Spherical quadrature formulas exact to orders 25−29. *Sib. Math. J.* **1977**, *18*, 99−107.
(34) Lebedev, V.; Skorokhodov, A. Quadrature formulas for a sphere of orders 41, 47, and 53. *Dokl. Akad. Nauk* **1992**, *324*, 519−524.
(35) Lebedev, V. A quadrature formula for the sphere of 59th algebraic order of accuracy. *Dokl. Akad. Nauk* **1994**, *338*, 454−456.
(36) Lebedev, V.; Laikov, D. Quadrature formula for the sphere of 131st algebraic order of accuracy. *Dokl. Akad. Nauk* **1999**, *366*, 741−745.
(37) Weigend, F. Accurate Coulomb-fitting basis sets for H to Rn. *Phys. Chem. Chem. Phys.* **2006**, *8*, 1057−1065.

(38) Whitten, J. Coulombic potential energy integrals and approximations. *J. Chem. Phys.* **1973**, *58*, 4496−4501.
(39) Dunlap, B.; Conolly, J. W. D.; Sabin, J. On some approximations in applications of Xα theory. *J. Chem. Phys.* **1979**, *71*, 3396−3402.
(40) Grimme, S.; Antony, J.; Ehrlich, S.; Krieg, H. A consistent and accurate *ab initio* parametrization of density functional dispersion (DFT-D) for the 94 elements H-Pu. *J. Chem. Phys.* **2010**, *132*, 154104.
(41) Grimme, S.; Ehrlich, S.; Goerigk, L. Effect of the damping function in dispersion corrected density functional theory. *J. Comput. Chem.* **2011**, *32*, 1456−1465.
(42) Brandenburg, J. G.; Bates, J. E.; Sun, J.; Perdew, J. P. Benchmark tests of a strongly constrained semilocal functional with a long-range dispersion correction. *Phys. Rev. B: Condens. Matter Mater. Phys.* **2016**, *94*, 115144.
(43) Radoń, M. Benchmarking quantum chemistry methods for spin-state energetics of iron complexes against quantitative experimental data. *Phys. Chem. Chem. Phys.* **2019**, *21*, 4854−4870.
(44) Kresse, G.; Hafner, J. Ab initio molecular dynamics for liquid metals. *Phys. Rev. B: Condens. Matter Mater. Phys.* **1993**, *47*, 558.
(45) Kresse, G.; Hafner, J. Ab initio molecular-dynamics simulation of the liquid-metal-amorphous-semiconductor transition in germanium. *Phys. Rev. B: Condens. Matter Mater. Phys.* **1994**, *49*, 14251.
(46) Kresse, G.; Furthmüller, J. Efficient iterative schemes for ab initio total-energy calculations using a plane-wave basis set. *Phys. Rev. B: Condens. Matter Mater. Phys.* **1996**, *54*, 11169.
(47) Kresse, G.; Furthmüller, J. Efficiency of ab-initio total energy calculations for metals and semiconductors using a plane-wave basis set. *Comput. Mater. Sci.* **1996**, *6*, 15−50.
(48) Blöchl, P. E. Projector augmented-wave method. *Phys. Rev. B: Condens. Matter Mater. Phys.* **1994**, *50*, 17953.
(49) Kresse, G.; Joubert, D. From ultrasoft pseudopotentials to the projector augmented-wave method. *Phys. Rev. B: Condens. Matter Mater. Phys.* **1999**, *59*, 1758.
(50) Hinz, J.; Karasiev, V. V.; Hu, S. X.; Zaghoo, M.; Mejía-Rodríguez, D.; Trickey, S. B.; Calderín, L. Fully consistent density functional theory determination of the insulator-metal transition boundary in warm dense hydrogen. *Phys. Rev. Res.* **2020**, *2*, 032065.
(51) Zhang, Y.; Zhang, W.; Singh, D. J. Localization in the SCAN meta-generalized gradient approximation functional leading to broken symmetry ground states for graphene and benzene. *Phys. Chem. Chem. Phys.* **2020**, *22*, 19585−19591.
(52) Casey, S. M.; Leopold, D. G. Negative ion photoelectron spectroscopy of Cr_2. *J. Phys. Chem.* **1993**, *97*, 816−830.
(53) Simard, B.; Lebeault-Dorget, M.-A.; Marijnissen, A.; ter Meulen, J. J. Photoionization spectroscopy of dichromium and dimolybdenum: Ionization potentials and bond energies. *J. Chem. Phys.* **1998**, *108*, 9668.
(54) Vancoillie, S.; Malmqvist, P. Å; Veryazov, V. Potential energy surface of the chromium dimer re-re-visited with multiconfigurational perturbation theory. *J. Chem. Theory Comput.* **2016**, *12*, 1647−1655.

https://dx.doi.org/10.1021/acs.jpca.0c08883
J. Phys. Chem. A 2020, 124, 9889−9894